Scientific Research Publishing

Journal of Flow Control, Measurement & Visualization, 2023, 11, 15-29
https://www.scirp.org/journal/jfcmv
ISSN Online: 2329-3330
ISSN Print: 2329-3322

Gas Temperature Distribution and Fluctuation in a Lab-Scale Fire Whirl

Mariko Watanabe, Koki Okamoto

Faculty of Science and Technology, Sophia University, Tokyo, Japan
Email: mariko_w@sophia.ac.jp

How to cite this paper: Watanabe, M. and Okamoto, K. (2023) Gas Temperature Distribution and Fluctuation in a Lab-Scale Fire Whirl. *Journal of Flow Control, Measurement & Visualization*, **11**, 15-29.
https://doi.org/10.4236/jfcmv.2023.112002

Received: November 21, 2022
Accepted: March 19, 2023
Published: March 22, 2023

Abstract

Fire whirls cause an increase in fire damage. This study clarified the unsteady behavior of fire whirls, considering that instantaneous changes in the temperature and flame shape of fire whirls can affect the damage to the surrounding area. Numerical simulations of a lab-scale flame that simulates a fire whirl were performed to investigate the changes in gas temperature and velocity fields under various fuel inflow velocities. The flow field was obtained by solving a continuity equation and a three-dimensional Navier-Stokes equation, and the turbulence was resolved using a large eddy simulation. A chemical equilibrium partially premixed combustion model was used, and radiation effects were considered. The time-averaged gas temperature distribution along the burner central axis revealed that the gas temperature decreased monotonically from upstream to downstream. The time-averaged velocity distribution along the burner central axis showed that the velocity decreased as one moved downstream, but the decrease was uneven. The time variation of the gas temperature demonstrated that the higher the fuel inflow velocity, especially near the burner, the greater the gas temperature flutter. Furthermore, the larger the fuel inflow velocity, the larger the flame swell and wobble. The results showed that the fuel inflow velocity affected temperature fluctuation and flame undulating movement.

Keywords

Fire Whirl, Numerical Simulation

1. Introduction

Fire whirls occasionally occur in large-scale fires and cause severe fire damage. Many researchers have conducted theoretical, numerical, and experimental studies on fire whirls, particularly on the correlation between flame height and es-

sential parameters. For example, Liu and coworkers measured the burning rate, flame height, velocity and temperature profiles, and other properties in a fixed-frame-type fire whirl plume. They proposed a correlation between the flame height of the fire whirls and the heat release rate and circulation [1] [2] [3] [4]. The flame height and flame shape of fire whirls could be predicted using Chuah *et al.*'s theoretical model, which included a heat-feedback mechanism from the flame to the fuel surface and diffusion-momentum-buoyancy effects [5] [6]. Hartl and Smits experimented with a small-scale fire whirl and dimensional analysis [7]. Their results showed that the nondimensional whirl height depends on the nondimensional circulation. The results of experiments, computational fluid dynamics, and theoretical analysis by Hayashi *et al.* showed a correlation between a fire whirl's flame height and its vortex parameters [8] [9]. Chow *et al.* experimentally studied internal fire whirls in a vertical shaft 15 m high with different ventilation conditions and derived a correlation between the flame height and fuel mass consumption [10]. Dobashi *et al.* studied the relationship between flame height and radiant heat of fire whirls through small- and middle-scale experiments [11]. In addition to research on flame height, there have been numerical studies focusing on the vorticity-buoyancy interaction [12] [13], studies on the interaction between the central fire whirl and peripheral flames [14], and analytical and experimental studies on the flame width of turbulent fire whirls [15].

Most of the above studies evaluated fire whirl characteristics such as flame height in terms of time averages. In fire whirls, however, the flame height fluctuates and the center of the whirl moves. And such unsteady behavior of fire whirl is thought to affect fire damage. Regarding the movement of fire whirl, studies have been conducted on fire whirls moving on a line fire [16] and the relationship between crosswind and fire whirl movement [17]. Furthermore, an experimental study of the horizontal wander of fire whirls has been conducted [18]. However, few studies deal mainly with fluctuations in physical quantities such as temperature and velocity or fluctuations in flame height. Therefore, we clarify the fluctuation of fire whirls and their mechanism. This study examines the temperature distribution and its fluctuation for a lab-scale fire whirl as a preliminary step. In this regard, experiments and numerical simulations were performed under the same conditions and compared to confirm the validity of the numerical simulations. The differences in the temperature and velocity fields inside the fire whirl caused by the various fuel inflow velocities were then explained using numerical simulations.

2. Calculation Method

2.1. Outline

In this study, a numerical analysis was conducted using ANSYS Fluent from ANSYS Inc. The calculation grids were generated using ICEM CFD (ANSYS Inc.). A continuity equation and a three-dimensional Navier-Stokes equation

were solved. Turbulence was solved using large eddy simulation (LES), and a chemical equilibrium partially premixed combustion model was employed. The governing equations were discretized using a finite volume method. The momentum equation was discretized using a bounded central differencing method, and the energy, reaction progress variable, and mixing fraction equations were discretized using a second-order upwind method. The radiative transfer equation was discretized using a first-order upwind method. The time discretization was based on an implicit scheme.

2.2. Continuity and Momentum Equations

The governing equations employed for LES are obtained by filtering the Navier-Stokes equations. A filter decomposes turbulent flow into a resolvable scale and a subgrid scale (SGS). A filtered variable (denoted by an overbar) is defined as follows:

$$\overline{\varphi}(\mathbf{x}) = \int_D \varphi(\mathbf{x}') G(\mathbf{x}, \mathbf{x}') \mathrm{d}\mathbf{x}', \tag{1}$$

where $\varphi(\mathbf{x})$ is the physical quantity defined at point $\mathbf{x}$ in the entire flow domain D. A box filter was used for filter function G. For the variable density flows, density-weighted averages or Favre averages (denoted by an overtilde) are introduced:

$$\tilde{\varphi} = \frac{\overline{\rho\varphi}}{\overline{\rho}}, \tag{2}$$

where ρ is the density. The continuity equation and the Navier-Stokes equation obtained after filtering are, respectively, as follows [19]:

$$\frac{\partial \overline{\rho}}{\partial t} + \frac{\partial (\overline{\rho}\tilde{u}_i)}{\partial x_i} = 0, \tag{3}$$

$$\frac{\partial (\overline{\rho}\tilde{u}_i)}{\partial t} + \frac{\partial (\overline{\rho}\tilde{u}_i\tilde{u}_j)}{\partial x_j} = \frac{\partial \breve{\sigma}_{ij}}{\partial x_j} - \frac{\partial \overline{p}}{\partial x_i} - \frac{\partial \tau_{ij}}{\partial x_j} + \overline{\rho} g_i, \tag{4}$$

where u_i is the velocity component in the i direction, p is the pressure, g_i is the gravitational acceleration, and $\breve{\sigma}_{ij}$ is the stress tensor due to molecular viscosity and is defined by

$$\breve{\sigma}_{ij} = \overline{\mu}\left(\frac{\partial \tilde{u}_j}{\partial x_i} + \frac{\partial \tilde{u}_i}{\partial x_j}\right) - \frac{2}{3}\overline{\mu}\left(\frac{\partial \tilde{u}_l}{\partial x_l}\right)\delta_{ij}, \tag{5}$$

where μ is the viscosity and δ_{ij} is the Kronecker delta. The SGS stress tensor, τ_{ij}, is expressed as

$$\tau_{ij} = \overline{\rho}\left(\widetilde{u_i u_j} - \tilde{u}_i\tilde{u}_j\right). \tag{6}$$

τ_{ij} is modeled through the SGS eddy viscosity, μ_{sgs}, as

$$\tau_{ij} - \frac{1}{3}\tau_{kk}\delta_{ij} = -2\mu_{sgs}\left(\tilde{S}_{ij} - \frac{1}{3}\tilde{S}_{kk}\delta_{ij}\right), \tag{7}$$

where $\tilde{S}_{ij}$ is the strain rate tensor of the resolved scales shown as

$$\tilde{S}_{ij} = \frac{1}{2}\left(\frac{\partial \tilde{u}_i}{\partial x_j} + \frac{\partial \tilde{u}_j}{\partial x_i}\right). \tag{8}$$

The term involving τ_{kk} can be added to the filtered static pressure term. μ_{sgs} is calculated using the Smagorinsky-Lilly model [19] expressed as

$$\mu_{sgs} = \bar{\rho} L_s^2 \left|\tilde{S}\right|, \tag{9}$$

where $\left|\tilde{S}\right| \equiv \sqrt{2\tilde{S}_{ij}\tilde{S}_{ij}}$ and L_s is the mixing length for SGSs calculated by

$$L_s = \min\left(\kappa d, C_s \Delta\right), \tag{10}$$

where $\kappa = 0.41$ is the von Kármán constant, d is the distance to the closest wall, and C_s is the Smagorinsky constant, which is set to 0.1 in this calculation. The local grid scale Δ is given by

$$\Delta = V^{1/3}, \tag{11}$$

where V is the volume of the computational cell.

2.3. Combustion Model

The combustion model was the chemical equilibrium partially premixed model [19] in ANSYS Fluent. The model assumes that the premixed flame front is infinitely thin. The composition of the burned gas was calculated assuming chemical equilibrium. A value of reaction progress variable indicated the flame brush, c, defined as

$$c = \frac{Y_{\text{fuel}} - Y_{\text{fuel,u}}}{Y_{\text{fuel,b}} - Y_{\text{fuel,u}}}, \tag{12}$$

where Y_{fuel} is the fuel mass fraction. The subscripts u and b indicate unburned and burned gases, respectively. When $c = 0$, the mixture is unburned; when $c = 1$, the mixture is burned.

Assuming an infinitely thin flame front, since only unburned and burned gases exist, density-weighted mean scalars, $\tilde{\phi}$, such as species mass fractions and temperature, are computed using the density-weighted mean reaction progress variable $\tilde{c}$ and the density-weighted probability density function of the mixture fraction f, written as $\tilde{p}(f)$ in the following [19] [20]:

$$\tilde{\phi} = \tilde{c}\int_0^1 \phi_b(f)\tilde{p}(f)\mathrm{d}f + (1-\tilde{c})\int_0^1 \phi_u(f)\tilde{p}(f)\mathrm{d}f, \tag{13}$$

where the $\phi_b(f)$ and $\phi_u(f)$ are the scalars of the burned and unburned gases, both of which are functions of f, respectively. The mixture fraction f is written as

$$f = \frac{Z_i - Z_{i,O}}{Z_{i,F} - Z_{i,O}}, \tag{14}$$

where Z_i is the elemental mass fraction for the ith element. The subscripts O and F represent the oxidizer and fuel flow at the inlet. The β-function PDF shape is assumed to be a function of the density-weighted mean mixture fraction, $\tilde{f}$, and the mixture fraction variance $\widetilde{f'^2}$.

The transport equations of the density-weighted mean mixture fraction, $\tilde{f}$, and $\tilde{c}$ are expressed as [20]

$$\frac{\partial}{\partial t}\left(\overline{\rho}\tilde{f}\right)+\nabla\cdot\left(\overline{\rho}\tilde{\mathbf{v}}\tilde{f}\right)=\nabla\cdot\left\{\left(\frac{k}{C_p}+\frac{\mu_t}{Pr}\right)\nabla\tilde{f}\right\}, \tag{15}$$

$$\frac{\partial}{\partial t}\left(\overline{\rho}\tilde{c}\right)+\nabla\cdot\left(\overline{\rho}\tilde{\mathbf{v}}\tilde{c}\right)=\nabla\cdot\left\{\left(\frac{k}{C_p}+\frac{\mu_t}{Sc_t}\right)\nabla\tilde{c}\right\}+\overline{\rho}\tilde{S}_c, \tag{16}$$

where $\mathbf{v}$ is the velocity vector, k is the laminar thermal conductivity of the mixture, C_P is the mixture-specific heat, Pr is the Prandtl number, which is set to 0.85, μ_t is the turbulent viscosity, Sc_t is the turbulent Schmidt number, which is set to 0.7, and $\tilde{S}_c$ is the reaction progress source term. The mean reaction rate is modeled as

$$\overline{\rho}\tilde{S}_c=\rho_u U_t\left|\nabla\tilde{c}\right|, \tag{17}$$

where ρ_u is the density of the unburned mixture and U_t is the turbulent flame speed, calculated from the Zimont turbulent flame speed closure model [19]. For LES, the transport equation of $\widetilde{f''^2}$ is not solved. Instead, it is modeled as

$$\widetilde{f''^2}=C_{\mathrm{var}}L_s^2\left|\nabla\tilde{f}\right|^2 \tag{18}$$

where C_{var} is constant and set to 0.5.

When nonadiabatic mixtures are considered, the burned scalar ϕ_b is also a function of enthalpy. Therefore, $\tilde{\phi}$ is expressed as [19]

$$\tilde{\phi}=\tilde{c}\int_0^1\phi_b\left(f,\tilde{H}\right)\tilde{p}(f)\mathrm{d}f+\left(1-\tilde{c}\right)\int_0^1\phi_u(f)\,\tilde{p}(f)\mathrm{d}f, \tag{19}$$

where $\tilde{H}$ is the density-weighted mean enthalpy. The transport equation for the $\tilde{H}$ is modeled as [19]

$$\frac{\partial}{\partial t}\left(\overline{\rho}\tilde{H}\right)+\nabla\cdot\left(\overline{\rho}\tilde{\mathbf{v}}\tilde{H}\right)=\nabla\cdot\left(\frac{k}{C_p}\nabla\tilde{H}\right)+\overline{\rho}\tilde{S}_h, \tag{20}$$

where $\tilde{S}_h$ is the source term due to radiation. This calculation employed a discrete ordinates radiation model [19] as a radiation model. Look-up tables can be generated based on $\tilde{f}$, $\widetilde{f''^2}$, $\tilde{c}$ and $\tilde{H}$ described above, and scalar quantities such as mass fraction and temperature can be obtained by referring to them.

$$\tilde{\phi}=\tilde{\phi}\left(\tilde{f},\widetilde{f''^2},\tilde{c},\tilde{H}\right) \tag{21}$$

2.4. Calculation Condition

Figure 1 shows the schematic of the computational domain. The computational domain size was identical to that of the experimental apparatus, with a base of 500 mm × 500 mm and a height of 1000 mm. Fuel flowed in from 24 nozzles, each 1 mm in diameter, on the bottom surface. Air flowed in at a constant velocity from two locations on the sides to generate a swirling flow. The air inlet size was 50 mm × 150 mm. ICEM CFD from ANSYS Inc. was used for mesh generation. The total number of meshes was approximately 320,000. Hybrid Initialization

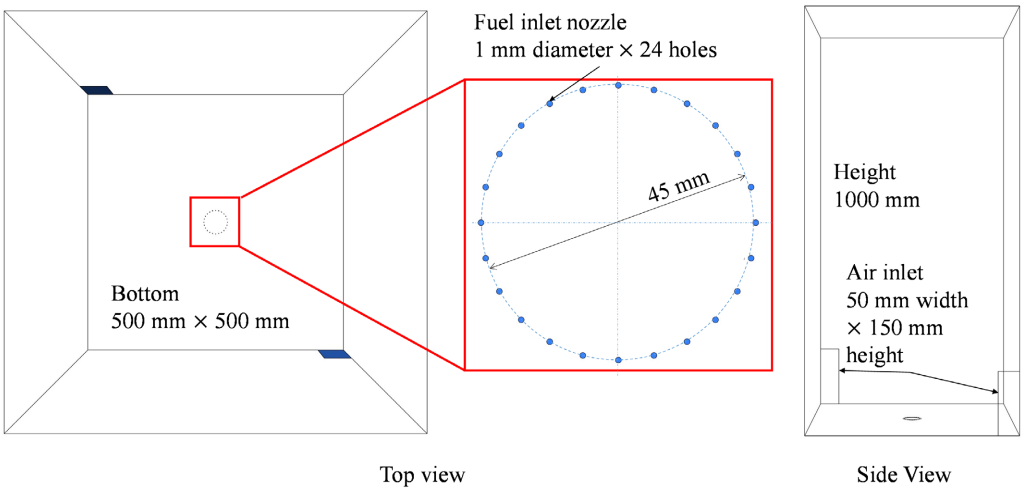

Figure 1. Schematic of the computational domain.

Table 1. Calculation conditions.

Fuel	Ethanol
Fuel temperature at the inlet	353 K
Air temperature at the inlet	300 K
Fuel inflow velocity	0.8, 1.2, 1.6 m/s
Air inflow velocity	2.5 m/s

in ANSYS Fluent [19] was used to initialize the entire flow field. The bottom and wall surfaces, except the fuel and air inlets, were subjected to a no-slip wall boundary condition at a temperature of 300 K. An outflow boundary condition was used for the upper part of the computational domain.

The conditions used in the numerical analysis are shown in Table 1. The fuel temperature at the inlet was set to the temperature at which ethanol volatilizes. Three cases were assumed for the fuel inflow velocity. The experiment's conditions were the same, with a fuel inflow velocity of 1.2 m/s. The fuel inflow velocity in the experiment was calculated from the fuel volume, time to burn off, and density ratio of liquid ethanol to ethanol vapor. The air inflow velocity of 2.5 m/s was the same as in the experiment. Additionally, air inflow velocities were calculated at 1.5 and 3.5 m/s. However, as these did not result in a fire whirl, only the results for 2.5 m/s were presented in this study. A 4-mm-diameter high-energy region was placed at the center of the bottom surface for 0 to 0.2 s to initiate the combustion reaction. For a total analysis duration of 60 s, the timesteps were totaled at 1200, and the time increments were set to 0.05 s. The number of iterations per time increment was 150.

3. Validation of Numerical Analysis

In this section, experiments were conducted to compare the numerical results and confirm the numerical methods' validity.

3.1. Experimental Setup

An alcohol burner (Trangia TR-B25) (Figure 2) was placed in the center of a table (Figure 3). The diameter of the fuel port of the burner was approximately 40 mm, and 24 small holes of 1 mm diameter were placed around the fuel port. Four partitions surrounded the 500-mm square table, and blowers blew the air through two of the 50-mm gaps between the partitions. Anhydrous ethanol was used as fuel. The flow velocity of the blower was measured using a hot wire anemometer (Anemomaster Lite Model 6006-D0, Kanomax Japan Inc.) and adjusted to 2.5 m/s. The temperatures in the flame were measured using a high-temperature sheath thermocouple type K (1SCHS1-0 K 0500 64 XL WXJ 003 AY, Chino Corporation). The time resolution of the thermocouple measurement was 2 s.

3.2. Generation of Lab-Scale Fire Whirl

The occurrence of a fire whirl in the experimental apparatus described above is shown in Figure 4. The figure from left to right shows how a flame developed into a fire whirl. A flame about 50 mm in height was observed immediately after ignition. The flame grew more significant with swirling and swellings and became a fire whirl about 500 mm high with a low, intense sound. The upper part of the fire whirl showed frequent large swells and fluctuations in height.

Figure 2. Alcohol burner.

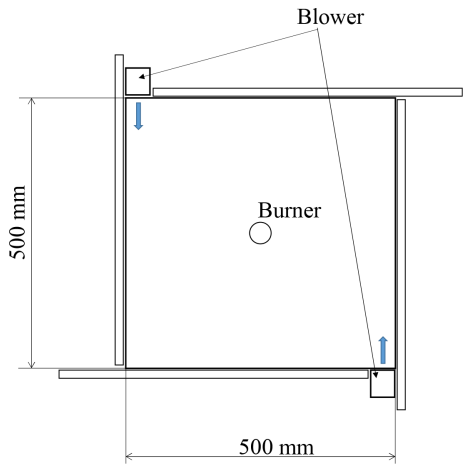

Figure 3. Schematic of the experimental setup.

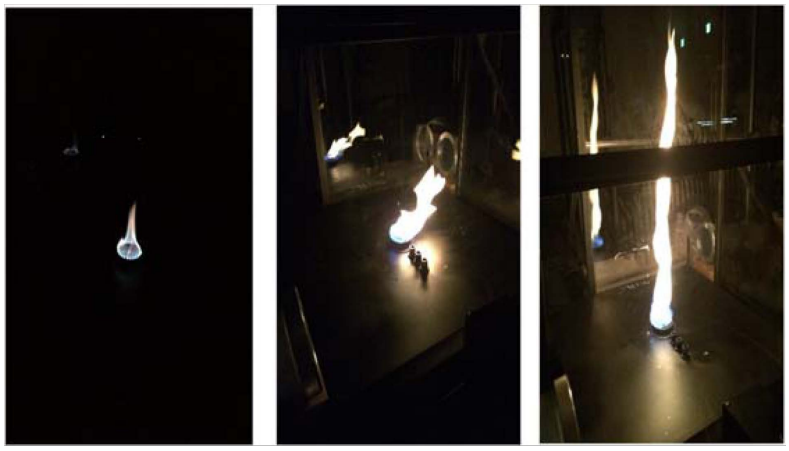

Figure 4. Transition to fire whirl.

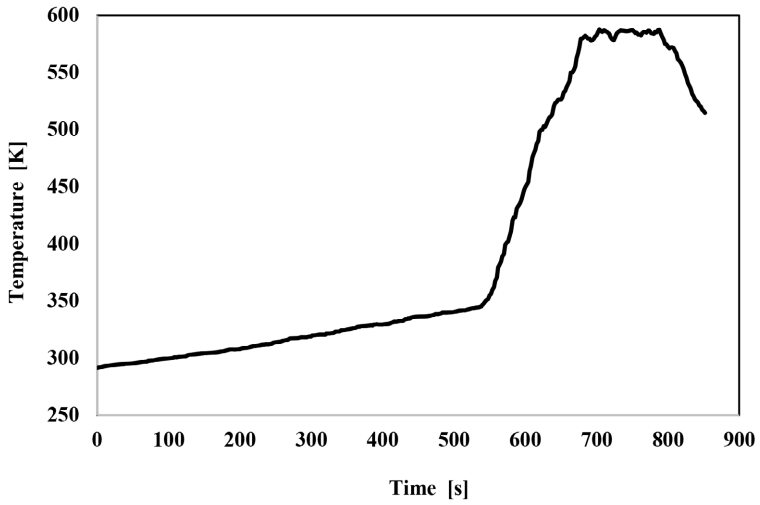

Figure 5. Temperature at a height of 200 mm from the top of the burner (on the burner's central axis).

3.3. Comparison of the Experimental and Numerical Results

By comparing the flame temperatures obtained from the experiments and numerical analysis, the validity of the numerical method was evaluated.

Figure 5 shows the measured temperature at the height of 200 mm from the top of the burner (on the burner's central axis). The burner was ignited at 0 s. A fire whirl formed at approximately 550 s, after which the temperature rose rapidly and converged to a constant value at approximately 700 s. When the fuel ran out and the fire whirl disappeared, the temperature rapidly decreased. The same trend was observed when the measurement height was changed. The experimental and numerical results for the temperature in the flame are compared in Figure 6. In the numerical analysis, the temperature values were averaged over the 40- to the 60-s period from the start of the calculation. In the experiment, the temperature values were averaged over a 100-s period, during which the gas temperature showed almost constant values. The graph also shows the maximum and minimum values. The difference between the maximum and mini-

mum values and the average is at most a dozen [K] and is barely visible on the graph because of the plot. By comparing the two, it can be observed that numerical analysis showed a higher gas temperature. This was because the time resolution of the experiment was 2 s and could not follow the rapid increase in gas temperature. In contrast, the numerical analysis captured the rapid increase in gas temperature. Although the difference between the two was about 20% at the height of 300 mm, there was the same tendency for the gas temperature to decrease as one moved downstream. Therefore, the flame structure may be evaluated using this numerical analytic technique.

4. Calculation Results and Discussion

4.1. Average Temperature and Velocity

Figure 7 shows the distribution of time-averaged gas temperature on the central axis between 40 and 60 s for three cases with different fuel inflow velocities. The

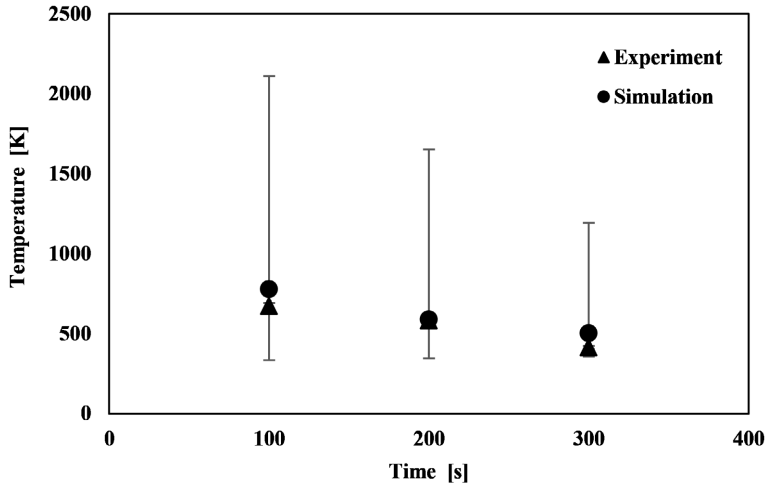

Figure 6. Comparisons of the experimental and numerical results for the gas temperature.

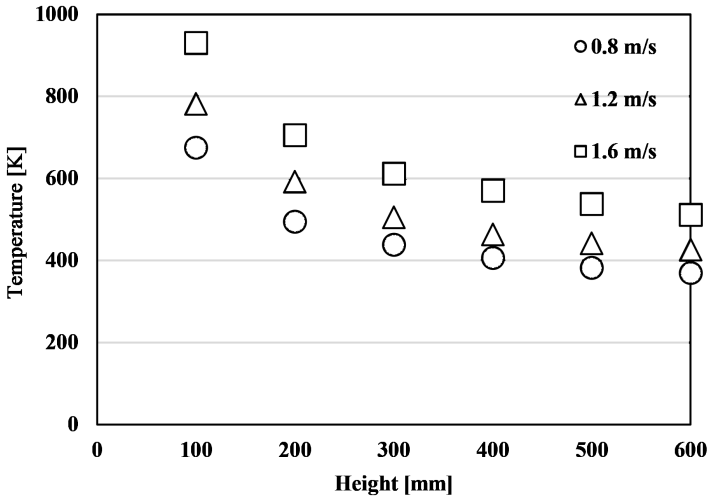

Figure 7. Comparison of the time-averaged gas temperature distribution on the central axis for different fuel inflow velocities.

average gas temperature was greater near the burner in all circumstances and dipped as the flow moved downstream. Also, the average gas temperature increased as the fuel inflow velocity increased. The distribution of the time-averaged velocity on the central axis between 40 and 60 s is shown in Figure 8. In the numerical simulation, the flow velocity near the bottom was minimal. It was not considered to match the actual phenomenon, so the results above the 300-mm height from the bottom were included in Figure 8. The velocity decreased at a constant rate for the fuel inflow velocities of 0.8 and 1.6 m/s as the flow proceeded downstream.

Meanwhile, for the 1.2 m/s, the velocity decreased relatively slowly between 300 and 500 mm and significantly between 500- and 600-mm. Figure 7 shows that the average gas temperature increased as the fuel inflow velocity increased, but the average flow velocity was higher for the 1.2-m/s case at the height of 500 mm. This irregularity, which is also explained in section 4.2, may be due to the undulation of the flame or a shift in the center position of the swirling flow.

4.2. Fluctuation of the Gas Temperature

The variations in gas temperature fluctuation at different fuel inflow velocities were studied. Figure 9 shows the time variation of the gas temperature between 40 and 60 s at the heights of (a) 100 mm, (b) 300 mm, and (c) 600 mm from the bottom. Figure 10 shows the standard deviation of the gas temperature's time variation. In Figure 9(a), the peak temperature value was almost the same at about 2000 K even when the fuel inflow velocity was changed, but there was a difference in the frequency of the peak occurrence. According to the peak temperature values, the temperature peak at this location could be inferred as due to the reaction zone passing through the observation point. In Figure 9(b), between 40 and 52 s, the gas temperature peaked above 1000 K for the fuel velocities of 1.2 and 1.6 m/s, and the flame temperature and its fluctuations were

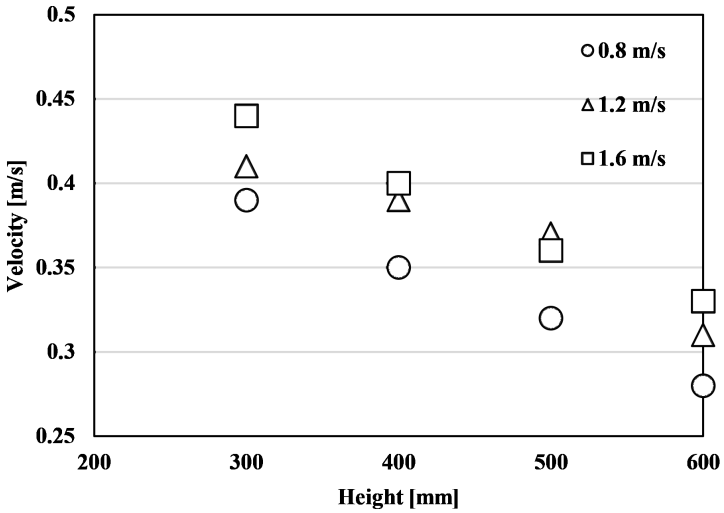

Figure 8. Comparison of the time-averaged velocity distribution on the central axis for different fuel inflow velocities.

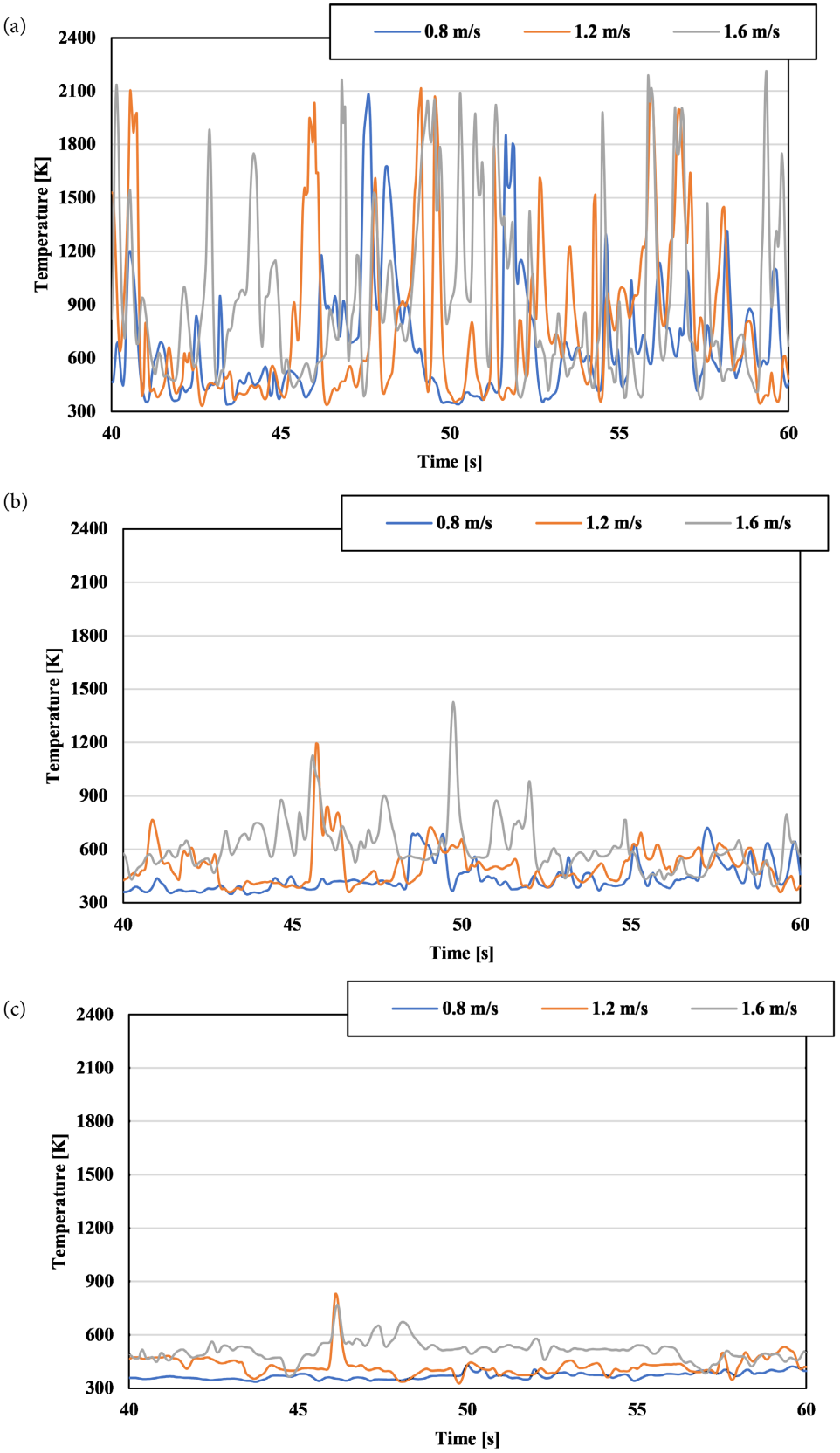

Figure 9. Time variation of the gas temperature between 40 and 60 s at the heights of (a) 100 mm, (b) 300 mm, and (c) 600 mm from the bottom.

slightly larger than those for the 0.8-m/s case. Meanwhile, there was no significant difference in all conditions after 52 s. Figure 10 shows that at the height of 300 mm, the standard deviation increased with the fuel inflow velocity, although it was only a few tens of K. In Figure 9(c), there is a clear peak around 46 s for the fuel flow velocities of 1.2 and 1.6 m/s, but overall, temperature fluctuations are small for all conditions. The standard deviations are slight for all conditions, as observed in Figure 10.

Figure 11 shows the temperature distribution when the fire whirl is stable, whereas Figure 12 shows the isosurface at a 500-K temperature. Figure 13 represents the velocity vector diagram in the horizontal plane at the height of 300 mm from the bottom at the same time as Figure 11 and Figure 12. The size and color of the arrows indicate the magnitude of the velocity. Although not readily apparent from this figure, the flow is three-dimensional, and has a velocity

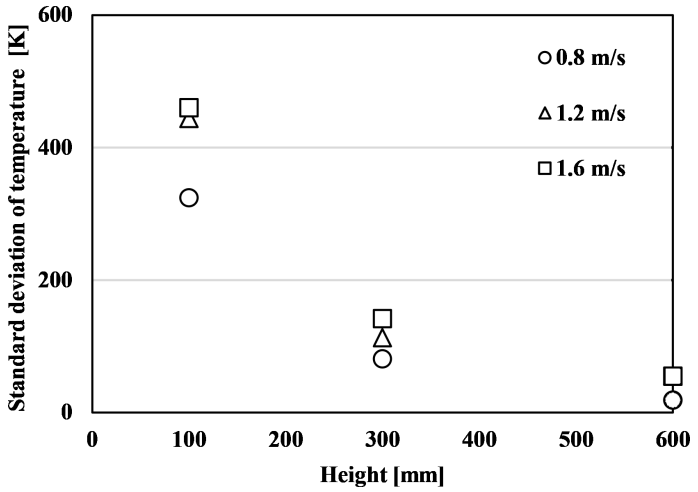

Figure 10. Standard deviation of the time variation of the gas temperature.

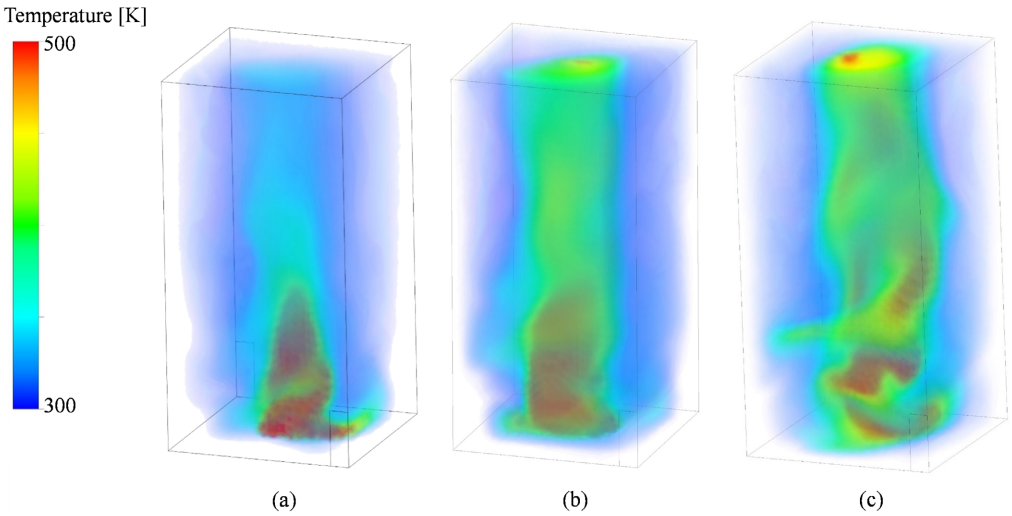

Figure 11. Temperature distribution when the fire whirl is stable: (a) fuel inflow velocity = 0.8 m/s, time = 48.75 s; (b) fuel inflow velocity = 1.2 m/s, time = 35.00 s; (c) fuel inflow velocity = 1.6 m/s, time = 39.75 s.

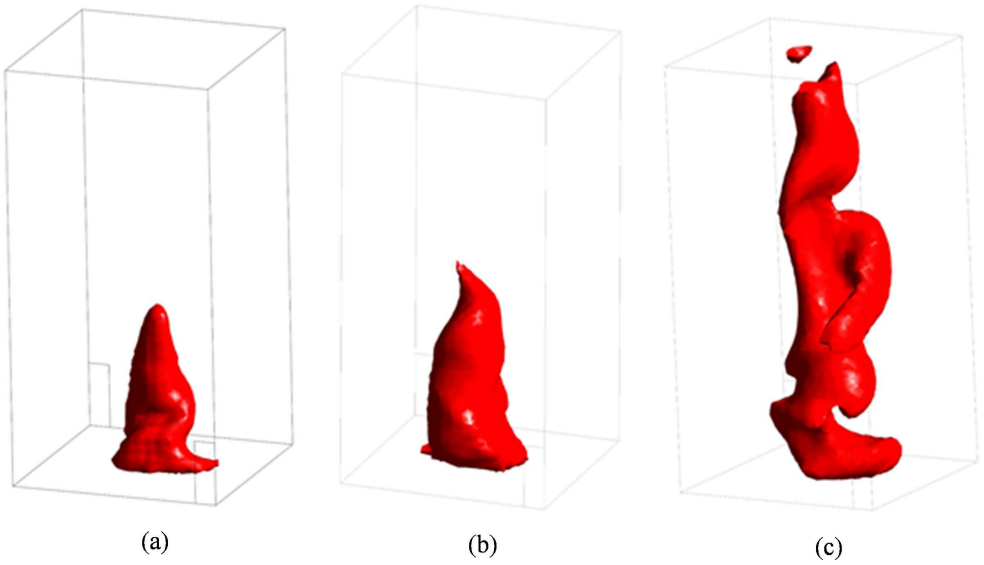

Figure 12. Isosurface at a 500-K temperature: (a) fuel inflow velocity = 0.8 m/s, time = 48.75 s; (b) fuel inflow velocity = 1.2 m/s, time = 35.00 s; (c) fuel inflow velocity = 1.6 m/s, time = 39.75 s.

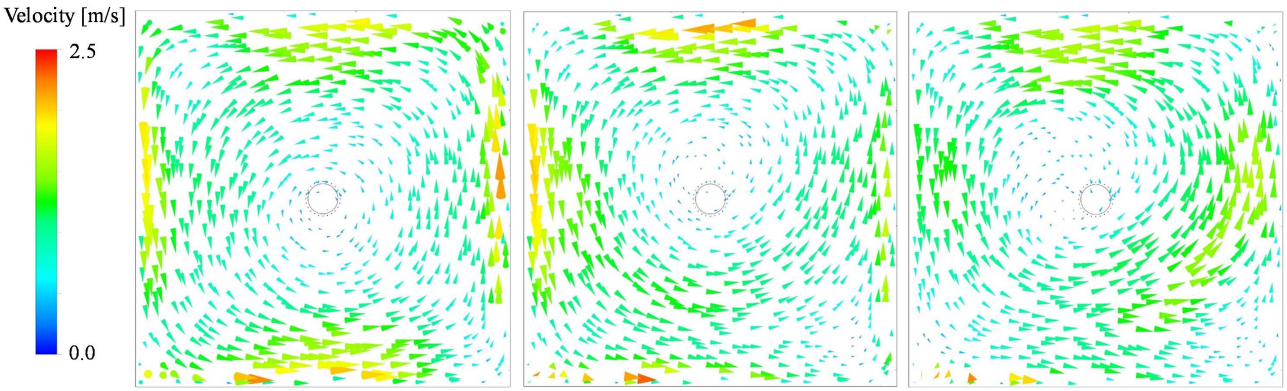

Figure 13. Velocity vector diagram in the horizontal plane at a height of 300 mm from the bottom: (a) fuel inflow velocity = 0.8 m/s, time = 48.75 s; (b) fuel inflow velocity = 1.2 m/s, time = 35.00 s; (c) fuel inflow velocity = 1.6 m/s, time = 39.75 s.

component perpendicular to the paper surface. As shown in Figure 11 and Figure 12, as the fuel inflow velocity increased, the temperature of the entire calculation region became higher, and the undulation and waviness of the flame increased. Consequently, a swirling flow can be observed in the horizontal plane, as shown in Figure 13. The velocity at the wall was zero because the no-slip boundary condition was applied, but the velocity was large near the wall and decreased toward the center of the turning. The center of the swirling flow is off the central axis of the burner, and the position of the center of the swirling flow varied with the height from the bottom and time, although the figure is omitted in this study. At the 300- and 600-mm heights from the bottom, the combustion reaction is considered to be almost complete based on their gas temperatures. Therefore, it is assumed that the gas temperature fluctuations at these sites are influenced by horizontal motions such as flame undulation and movement of

the center of the swirling flow, as shown in Figure 11 to Figure 13, in addition to the effects of flame fluctuations upstream.

5. Conclusion

To investigate the transient behavior of fire whirls, we performed an LES that can numerically analyze lab-scale fire whirls and confirmed its accuracy by comparing numerical results with experimental results. Then numerical simulations were performed to investigate the changes in temperature and velocity fields in the fire whirl under various fuel inflow velocities. The time-averaged gas temperature distribution along the burner's central axis showed that the gas temperature monotonically decreased from upstream to downstream. Additionally, the higher the fuel inflow velocity is, the higher the gas temperature is. The distribution of time-averaged velocity along the burner's central axis showed that the velocity decreased as one moved downstream; however, the decrease was not uniform, and there was a gradual decrease at a fuel inflow velocity of 1.2 m/s. Then, we examined the time variation of the gas temperature and found that the larger the fuel inflow velocity, the greater the flutter of the gas temperature, especially near the burner. The visualization results of the gas temperature distribution showed that the larger the fuel inflow velocity, the larger the flame swell and wobble. The results showed that the fuel inflow velocity affected temperature fluctuation and flame undulating movement. This study enabled simulations that captured the fluctuation of fire whirls. In the future, while conducting experiments in parallel, we will investigate the characteristics of flame height fluctuations and clarify the relationship between various parameters and fluctuation characteristics.

Conflicts of Interest

The authors declare no conflicts of interest regarding the publication of this paper.

References

[1] Lei, J., Liu, N., Zhang, L., Chen, H., Shu, L., Chen, P., Deng, Z., Zhu, J., Satoh, K. and Ris, J.L. (2011) Experimental Research on Combustion Dynamics of Medium-Scale Fire Whirl. *Proceedings of the Combustion Institute*, **33**, 2407-2415. https://doi.org/10.1016/j.proci.2010.06.009

[2] Zhou, K., Liu, N., Lozano, J.S., Shan, Y., Yao, B. and Satoh, K. (2013) Effect of Flow Circulation on Combustion Dynamics of Fire Whirl. *Proceedings of Combustion Institute*, **34**, 2617-2624. https://doi.org/10.1016/j.proci.2012.06.053

[3] Lei, J., Liu, N., Zhang, L. and Satoh, K. (2015) Temperature, Velocity and Air Entrainment of Fire Whirl Plume: A Comprehensive Experimental Investigation. *Combustion and Flame*, **162**, 745-758. https://doi.org/10.1016/j.combustflame.2014.08.017

[4] Wang, P., Liu, N., Hartl, K. and Smits, A. (2016) Measurement of the Flow Field of Fire Whirl. *Fire Technology*, **52**, 263-272. https://doi.org/10.1007/s10694-015-0511-0

[5] Chuah, K.H. and Kushida, G. (2007) The Prediction of Flame Heights and Flame Shapes of Small Fire Whirls. *Proceedings of the Combustion Institute*, **31**, 2599-2606. https://doi.org/10.1016/j.proci.2006.07.109

[6] Chuah, K.H., Kuwana, K. and Saito, K. (2009) Modeling a Fire Whirl Generated over a 5-cm-Diameter Methanol Pool Fire. *Combustion and Flame*, **156**, 1828-1833. https://doi.org/10.1016/j.combustflame.2009.06.010

[7] Hartl, K.A. and Smits, A.J. (2016) Scaling of a Small Scale Burner Fire Whirl. *Combustion and Flame*, **163**, 202-208. https://doi.org/10.1016/j.combustflame.2015.09.027

[8] Hayashi, Y., Kuwana, K. and Dobashi, R. (2011) Influence of Vortex Structures on Fire Whirl Structure. *Fire Safety Science*, **10**, 671-679. https://doi.org/10.3801/IAFSS.FSS.10-671

[9] Hayashi, Y., Kuwana, K., Mogi, T. and Dobashi, R. (2013) Influence of Vortex Parameters on the Flame Height of a Weak Fire Whirl via Heat Feedback Mechanism. *Journal of Chemical Engineering of Japan*, **46**, 689-694. https://doi.org/10.1252/jcej.13we078

[10] Chow, W.K., He, Z. and Gao, Y. (2011) Internal Fire Whirls in a Vertical Shaft. *Journal of Fire Sciences*, **29**, 71-92. https://doi.org/10.1177/0734904110378974

[11] Dobashi, R., Okura, T., Nagaoka, R. Hayashi, Y. and Mogi, T. (2016) Experimental Study on Flame Height and Radiant Heat of Fire Whirls. *Fire Technology*, **52**, 1069-1080. https://doi.org/10.1007/s10694-015-0549-z

[12] Battaglia, F., Rehm, R.G. and Baum, H.R. (2000) The Fluid Mechanics of Fire Whirls: An Inviscid Model. *Physics of Fluids*, **12**, 2859-2867. https://doi.org/10.1063/1.1308510

[13] McDonough, J.M. and Loh, A. (2003) Simulation of Vorticity-Buoyancy Interactions in Fire-Whirl-Like Phenomena. *Proceedings of ASME Summer Heat Transfer Conference*, Las Vegas, NV, USA, 21-23 July 2003, 195-201. https://doi.org/10.1115/HT2003-47548

[14] Zhou, R. and Wu, Z.-N. (2007) Fire Whirls due to Surrounding Flame Sources and the Influence of the Rotation Speed on the Flame Height. *Journal of Fluid Mechanics*, **583**, 313-345. https://doi.org/10.1017/S0022112007006337

[15] Lei, J., Huang, P., Liu, N. and Zhang, L. (2022) On the Flame Width of Turbulent Fire Whirls. *Combustion and Flame*, **244**, Article No. 11285. https://doi.org/10.1016/j.combustflame.2022.112285

[16] Kuwana, K., Sekimoto, K., Minami, T., Tashiro, T. and Saito, K. (2013) Scale-Model Experiments of Moving Fire Whirl over a Line Fire. *Proceedings of the Combustion Institute*, **34**, 2625-2631. https://doi.org/10.1016/j.proci.2012.06.092

[17] Zhou, K., Liu, N., Yin P., Yuan, X. and Jiang J. (2014) Fire Whirl due to Interaction between Line Fire and Cross Wind. *Fire Safety Science*, **11**, 1420-1429. https://doi.org/10.3801/IAFSS.FSS.11-1420

[18] Wang, P., Liu, N., Liu, X. and Yuan X. (2018) Experimental Study on Flame Wander of Fire Whirl. *Fire Technology*, **54**, 1369-1381. https://doi.org/10.1007/s10694-018-0734-y

[19] ANSYS, Inc. (2020) ANSYS Fluent Theory Guide. ANSYS Inc., Canonsburg.

[20] Pierce, C.D. and Moin, P. (2004) Progress-Variable Approach for Large-Eddy Simulation of Non-Premixed Turbulent Combustion. *Journal of Fluid Mechanics*, **504**, 73-97. https://doi.org/10.1017/S0022112004008213